Nuclear Engineering and Technology 54 (2022) 1024–1029

Contents lists available at ScienceDirect

Nuclear Engineering and Technology

journal homepage: www.elsevier.com/locate/net

Original article

GYAGG/^{6}LiF composite scintillation screen for neutron detection

A. Fedorov [a, b], I. Komendo [b, c], A. Amelina [b, c], E. Gordienko [b, c], V. Gurinovich [d], V. Guzov [d], G. Dosovitskiy [b, c], V. Kozhemyakin [d], D. Kozlov [a], A. Lopatik [d], V. Mechinsky [a, b], V. Retivov [b, c], V. Smyslova [c], A. Zharova [c], M. Korzhik [a, b, *]

[a] Institute for Nuclear Problems of Belarus State University, Minsk, Belarus
[b] NRC "Kurchatov Institute", Moscow, Russia
[c] NRC "Kurchatov Institute" - IREA, Moscow, Russia
[d] ATOMTEX SPE, Minsk, Belarus

ARTICLE INFO

Article history:
Received 21 May 2021
Received in revised form
17 August 2021
Accepted 22 September 2021
Available online 25 September 2021

Keywords:
Neutron
Gadolinium
Lithium
Scintillator
Detector
Screen

ABSTRACT

Composite scintillation screens on a base of $Gd_{1.2}Y_{1.8}Ga_{2.5}Al_{2.5}O_{12}$:Ce (GYAGG) scintillator have been evaluated for neutron detection. Besides the powdered scintillator, the composite includes ^{6}LiF particles; both are merged with a binder and deposited onto the light-reflecting aluminum substrate. Results obtained demonstrates that screens are suitable for use with a silicon photomultiplier readout to create a prospective solution for a compact and low-cost thermal neutron sensor. Composite GYAGG/^{6}LiF scintillation screen shows a pretty matched sensitivity and γ-background rejection with a widely used ZnS/^{6}LiF screens however, possesses forty times faster response.

1. Introduction

In the field of thermal neutron detection, ZnS:Ag polycrystalline phosphor is widely used due to high ZnS light yield under α-particles. It is utilized for the construction of large-area neutron detector screens, which may be read out with the assistance of high aperture optics by relatively small photodetectors, e.g. photomultiplier tubes PMTs or charge coupled device CCD camera [1]. Such detector screen normally consists of mixture of ZnS:Ag and ^{6}LiF particles [2], or sole Gd_2O_2S:Tb (GOS) [3] bonded with a binder and deposited onto a substrate. Detection of neutrons is based on neutron reactions with ^{6}Li nuclei ^{6}Li(n, α)T: ^{6}Li+n-> α+$^{3}_{1}$H, where an α-particle and a nucleus of tritium (Triton) have energy 2.05 and 2.73 MeV correspondingly. To date, the scintillation yield of ZnS:Ag has been estimated over a wide range. According to Ref. [4], a number of scintillation photons emitted per an absorbed neutron from ZnS:Ag in the composite with ^{6}LiF reach 160000 and 55000 ph per one Mev of the α-particle. Authors [5] declared the typical Light Yield (LY) was 50000 ph/MeV, whereas ZnS:Ag LY under α-particles was 130% of NaI:Tl [6], which has light yield of 38000 ph/MeV under γ -excitation [7], or 49400 ph/MeV. No information on the LY of the scintillator under irradiation with tritons was announced yet. The scintillation kinetics of ZnS:Ag is still under debates since the first application of the material for neutron detection [8]. A recent study demonstrated domination of the relatively slow decay time components in a range of a few microseconds [9]. Nevertheless, the material was found to be capable to operate with fast silicon photomultipliers (SiPMs) [10].

Among a variety of scintillation materials [11], garnets type crystalline compounds, which found a great application in solid-state lighting [12] as well, can be the prospective candidates to creating composite neutron sensitive screens. The basic $Y_3Al_5O_{12}$:Ce scintillator has a relatively low light yield in a comparison with novel alkali halide scintillators like $LaBr_3$:Ce [13,14] or SrI_2:Eu [15,16], which, however demonstrate a strong hygroscopicity and are useless to manufacture scintillation screens. Mixed Al/Ga garnets manifest better light yield in a crystalline form [17,18]. Recently we demonstrated that a transfer from ternary to quaternary garnets, in which a part of Gd ions is substituted with Y, results

* Corresponding author. Institute for Nuclear Problems of Belarus State University, Minsk, Belarus.
E-mail address: mikhail.korjik@cern.ch (M. Korzhik).

https://doi.org/10.1016/j.net.2021.09.024

in an increase of the LY [19,20] both under γ-quanta and α-particles excitation. This finding put forward an application of these materials to construct scintillation screens. Quaternary garnets in a crystalline form with the optimized ratio between the Y, Gd, Al, Ga cations in the composition can be obtained by a variety of methods, from crystal growth [21,22] to coprecipitation and a typical route for ceramics [23].

Scintillation properties of some of the garnet type crystals doped with Ce are summarized in Table 1.

Incorporation of Gd into the scintillator results in a larger sensitivity to γ-quanta, however, a gadolinium natural isotopic composition has the thermal neutron's absorption cross-section of 49000 barns, mainly due to radiation capture (n,γ) reaction. This feature was exploited recently to show a good potential of the GAGG scintillator to detect neutrons in a wide energy range [25–27]. It was shown that ~40% of counts in the amplitude spectrum at the radiation capture of slow neutrons may be under the 77 keV peak in γ-spectrum, which, in turn, is a sum of the energy deposit of Gd Kα photon and an internal conversion electron. In our study we evaluated an advantage of the combining of the Gd high light yield scintillator and ^{6}LiF absorber. Both species generate under neutrons the secondaries, which have short trajectories after being emitted. This might promote a better sensitivity of the composite to the neutrons in a thinner layer.

2. Material and methods

To optimize parameters of the particles to be included into the composite, the GEANT 4 simulation has been performed. It included consideration within the spherical model the pathlengths of the α-particles (E_α = 2,05 MeV) and tritons (E_T = 2,73 MeV) in the different components of the composite and an optimization of the energy losses of the secondaries in the scintillator particles. At the modelling, a hypothetic source emitting 10^6 particles of the secondaries was placed in the middle of the sphere consisted of ^{6}LiF (ρ = 2,64 g/cm^3), or GYAGG (ρ = 6,0 g/cm^3). Fig. 1 and Fig. 2 show simulated distributions of α-particle and Triton pathlengths (distances between the center of sphere and stop-point) in ^{6}LiF and GYAGG.

It was found that in both media the pathlength of tritons is about 6 times higher. Another finding is that 10–15 μm size of GYAGG particle is enough to absorb all products in ^{6}Li(n, α)T reaction. A significant part of the low energy secondaries to be produced at the neutron Gd radiation capture will be absorbed in the particles of a such size as well.

The secondaries lose kinetic energy in ^{6}Li particles and binder as well. The residual kinetic energy causes the energy deposition in the particles of the scintillator. The energy losses of α-particle and Triton after passing layers with different thicknesses of ^{6}LiF and a binder are in Fig. 3. A binder at the modelling was Huntsman TDR 1100 epoxy resin [28].

As seen, an optimal lithium fluoride grain size providing the minimal energy losses of secondaries should not exceed 1–2 μm. At such conditions a significant part of their energy may be delivered to the scintillator particles. Apparently, a smaller ^{6}LiF particles size is even better, however, their optimal size is a result of the trade-in

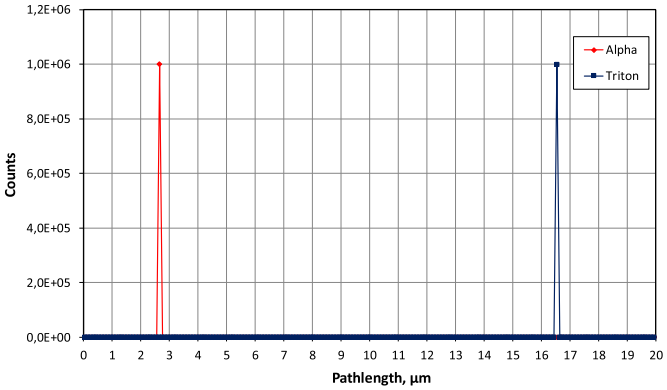

Fig. 1. Simulated α-particle and Triton pathlength distributions in ^{6}LiF.

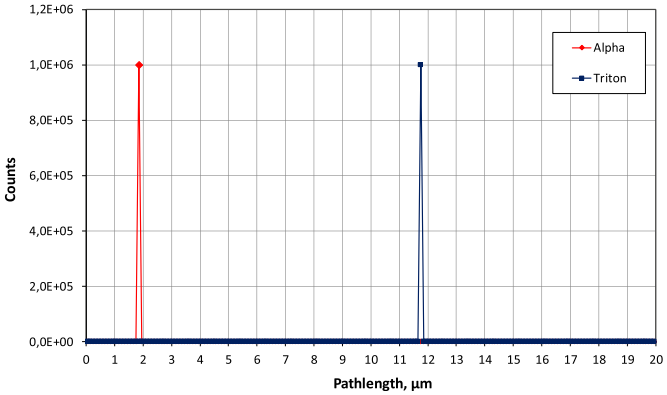

Fig. 2. Simulated α-particle and Triton pathlength distributions in GYAGG.

between minimal energy losses of the secondaries and growing light scattering effects by particles close in dimension to the light wavelength. Energy losses in the binder are smaller to ^{6}LiF. Thus, an average distance between ^{6}LiF and GYGG grains, which will be filled with the binder, might be in a range of 3–4 μm. Based on simulations we engineered composites at the thickness of 200–300 μm, which provide stopping power to thermal neutrons at the level of 50%. In the composite developed we expected that tritons will play a primary role in the exciting of the scintillator particles.

To produce composites a GYAGG scintillation pigment in a powdered form was prepared. A first step, $Gd_{1.2}Y_{1.8}Al_{2.5}Ga_{2.5}O_{12}$:Ce powder was prepared by precipitation of mixed metals nitrate solution by ammonia hydrocarbonate. Carbonate precipitate was calcined at 850°C during 2 h and milled in Retsch PM100 planetary mill in isopropanol media. For preparing the $Gd_{1.2}Y_{1.8}Al_{2.5}Ga_{2.5}O_{12}$:Ce ceramics, calcined at 850°C powder was compacted in tablets by uniaxial pressing under 64 MPa and sintered at 1700°C during 4 h in an oxygen atmosphere. After sintering ceramics tablets had ~94% of theoretical density. Then, tablets were grinded in a Retsch BB50 jaw crusher to a particle size of ~100 μm. The fraction was further milled in the planetary mill with a citrate mixture as a dispersant. The required fraction of the scintillation

Table 1
Properties of cerium activated garnet scintillators in a crystalline form.

Scintillator	Density, g/cm^3	Light yield under γ(α) excitation, ph/MeV	Scintillation decay time, ns	Scintillation wavelength maximum, nm	Ref.
$Y_3Al_5O_{12}$:Ce	4.55	30000 (6000)	~100	550	[24]
$Gd_3Al_2Ga_3O_{12}$:Ce	6.67	41000 (8000)	80	520	[19]
$Gd_{1.5}Y_{1.5}Ga_3Al_2O_{12}$:Ce	5.86	52000 (12500)	48	510	[19]

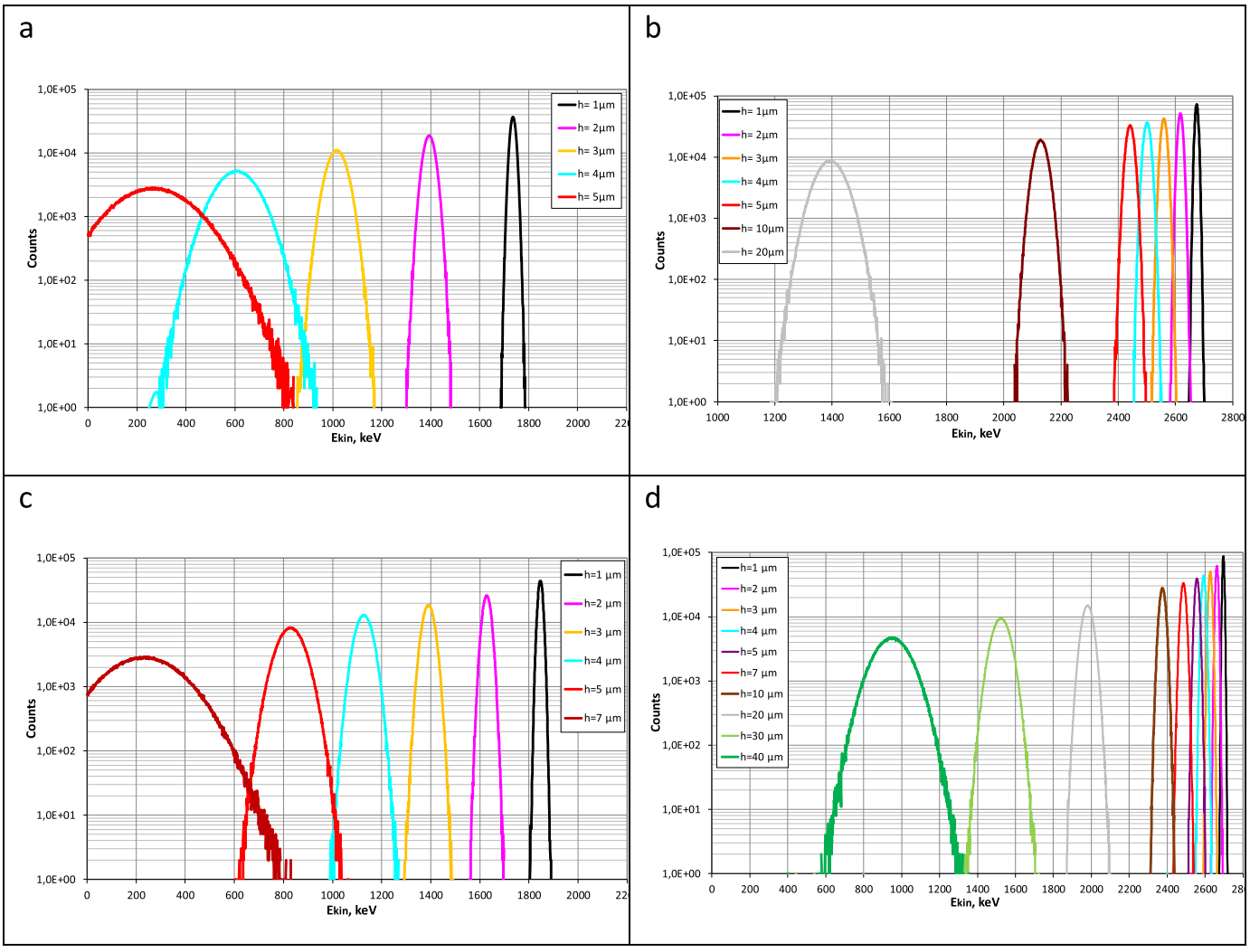

Fig. 3. Residual energy spectra of α-particles (a,c) and tritons (b,d) after passing through ^{6}LiF (first raw) and a binder (second raw) layers of different thick (indicated in the inset).

pigment was obtained by decanting a fine fraction of an aqueous suspension and sieving the dry residue through a sieve with a mesh size of 40 μm. The same procedure was applied to a single crystal $Gd_{1.5}Y_{1.5}Al_2Ga_3O_{12}$:Ce, which was cut from the same ingot as described in Ref. [19]. Particle size distribution of scintillation powders was evaluated on MALVERN MASTERSIZER 2000 using laser diffraction method and is shown in Fig. 4(a). Powder microstructure was characterized using Scanning Electron Microscope (SEM) Hitachi SU5100. SEM images of the typical particles of milled single crystal and ceramics are in Fig. 4(b,c).

LiF or ^{6}LiF absorber particles were prepared by dissolving $^{6}Li_2CO_3$ in diluted sulfuric acid and then obtained $^{6}Li_2SO_4$ solution was added by droplets into HF+NH_4F mixture. Lithium fluoride precipitate was washed, dried, and calcined at 500°C. The required fraction of ^{6}LiF was obtained by the similar procedure described above for milled ceramics powder.

We used aluminum substrates for composite layer and prepared them before coating as follows: 12x12 substrates were etched by 5% phosphoric acid solution for 24 h to form a thin hydrophilic $AlPO_4$ layer on the surface. Aluminum substrates were rigorous washed

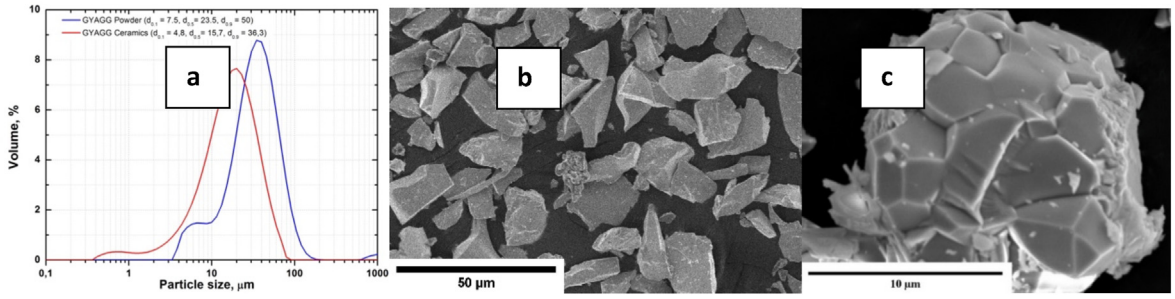

Fig. 4. Particle size distribution (a) and SEM image (b) for the scintillation pigment produced from a single crystal (b) and ceramics (c).

after acid treatment by deionized water with specific resistivity ≥18 MOhm and dried under dust-free conditions. Fig. 5 shows a SEM image of the Z-cut of the composite layer.

Samples, which contained unenriched LiF particles were evaluated with ^{241}Am (10^4Bq) α-particle source as described in Ref. [29], Fig. 6 shows a comparison of the response of samples prepared with pigments of milled ceramics and single crystal of GYAGG scintillator. The compositions were highly filled with pigments ~90% by volume, which results in a density of ~50 mg/cm^2. As a reference, we used a 12 × 12 mm piece of Scintacor ND neutron screen (ND screen) [30]. The measurements were performed with HAMAMATSU R339 PMT in 45° geometry from the surface bombarded by α-particles of the source. Amplitude spectra of the samples in a comparison with the reference are in Fig. 6.

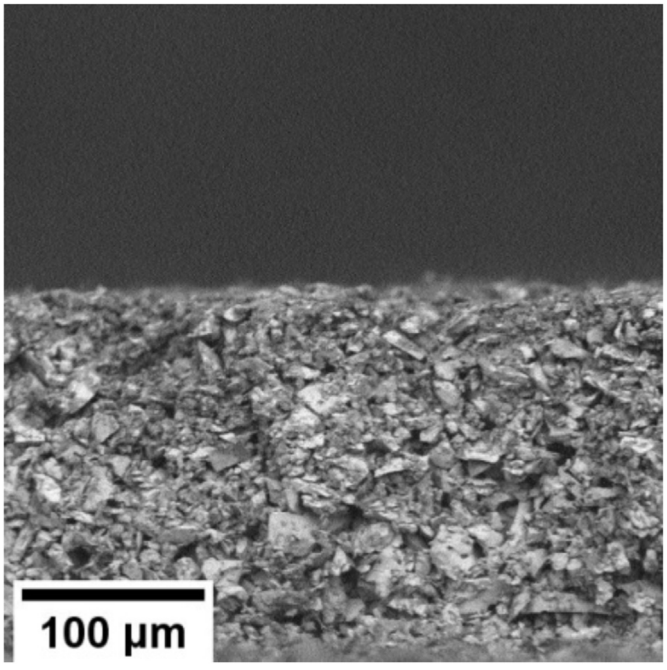

Fig. 5. Cross-section of the screen made with a milled single crystal pigment, observed by SEM.

Both samples based on GYAGG pigments demonstrates distinct full-absorption peaks of the α-particles. Peak positions were estimated to be ~900 channel for ND screen, and in 111 and 229 channels for GYAGG milled ceramics and crystal correspondingly. Through ZnS:Ag light yield is 49400 ph/MeV under α-particles, one can conclude that light output of samples made of GYAGG milled ceramics and the crystal was found to be 9700 ph/MeV and 12500 ph/MeV respectively. It indicates that light collection efficiency from composites developed is pretty similar to that of crystalline samples (Table 1). It is Worth noting, α-particle reveal distinct peaks in pulse height spectra in a comparison with a wide structureless response of the reference screen material, moreover, a high energy shoulder is detected due to double coincidences.

3. Results

For the tests with neutrons, samples were prepared with the utilization of ^{6}LiF(90% enrichment). Following the simulations, the screen composition consisted of ~10% vol. of scintillator, ~30% vol. of ^{6}LiF and 60% vol. of binder (GYAGG 10/30/60) has been prepared. The layer's density was identified to be 20 mg/cm^2.

Spectra under neutron and γ-quanta excitation were recorded with GYAGG 10/30/60 and reference sample at ATOMTEX SPE research facilities based on Pu–Be source. Source has 1 m distance to the sample. At such a distance the flux of neutrons was 0.6n/cm^2 per second. In addition, source was separated from the samples mounted on HAMAMATSU R339 PMT window without optical coupling grease with a 30 mm of polyamide moderator and 10 mm Pb/Cu absorber. Integration time at the registration was chosen to be 70 μs. Afterwards, the neutron source was replaced by a ^{137}Cs source with activity 10^5Bq having distance from not shielded by Pb/Cu absorber screen 20 mm. Acquisition time was 600 s in all cases. Fig. 7 represents a pulse height spectra of Pu–Be neutron source recorded with GYAGG 10/30/60 sample in a comparison with the reference.

One can conclude that the neutron sensitivity of GYAGG 10/30/60 and reference screen samples coincide to within the statistical error: the total number of counts from GYAGG 10/30/60 and

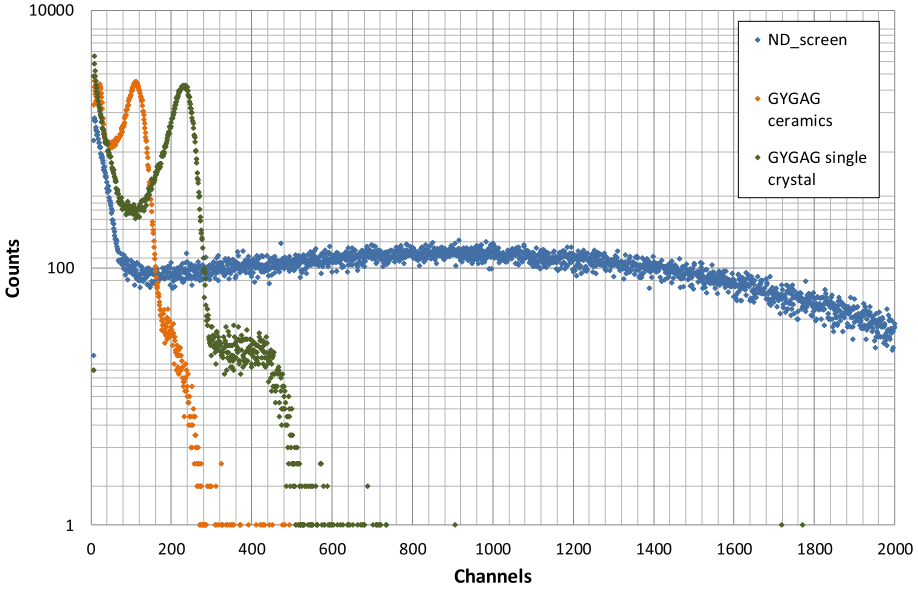

Fig. 6. Pulse height spectra of studied samples in a comparison with reference. In spectra measured with GYAGG one can see weak peaks of double coincidences.

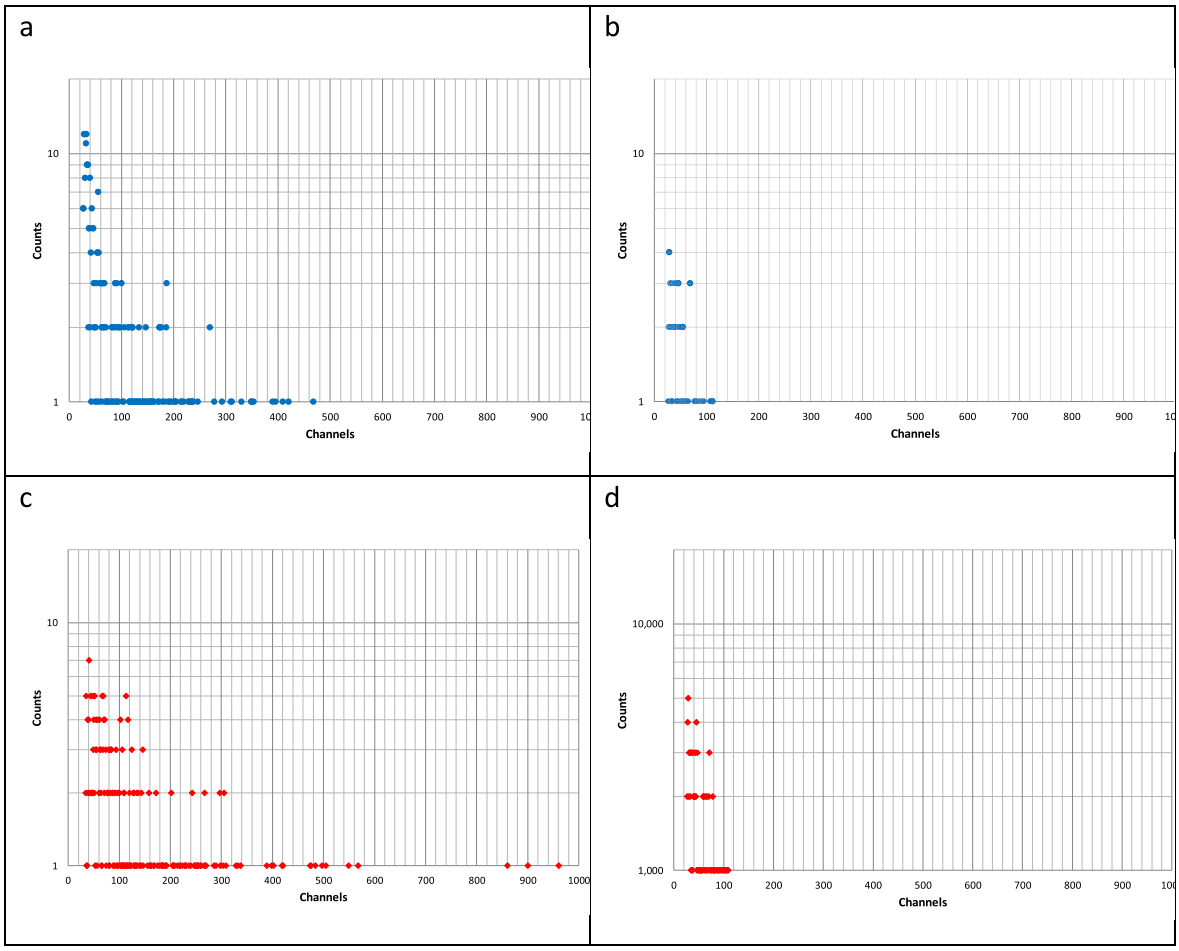

Fig. 7. Pulse height spectra GYAGG 10/30/60 (a,b) and reference sample ND screen(c,d) under Pu–Be neutron source and ^{137}Cs source respectively.

reference samples in neutron spectra (Fig.7 (a,c) are 321 and 299 respectively. Fig. 7(b,d) demonstrate that the γ-sensitivity is also rather close in both screens.

4. Discussion

Fig. 6 displays that GYAGG pigment-based screens with relatively high density show light output five times smaller under α-particle. However, GYAGG 10/30/60 screen, having density two times less, exhibits a light yield of ~40–50% of that of reference under neutrons. This result is achieved mainly due to the effective collection of Triton's energies, since for a single-charged particle a gamma-triton ratio of responses is expected to be much closer to 1 in GYAGG. Chosen mean distances between small ^{6}LiF particles and GYAGG grains possesses an effective Triton energy delivery to scintillation centers, even at the cost of unavoidable decrease of efficiency of α-particle's energy collection.

5. Conclusion

Neutron-sensitive screens utilizing $Gd_{1.2}Y_{1.8}Ga_{2.5}Al_{2.5}O_{12}$:Ce scintillation pigment have been developed. The composition of the screens includes pigment and ^{6}LiF particles, which are conjucted by the binder and mounted on the substrate. The developed screen demonstrates a similar count rate of the neutrons as a reference ND type screen. Furthermore, it is capable to exhibit γ-quanta rejection close to that of ZnS:Ag screen. Moreover, GYAGG/^{6}LiF possesses a forty times faster response, which allows operating with high fluxes of the neutrons. The potential for further improvement of the GYAGG based screen response is bound to the improvement of the light extraction from the scintillation pigment particles. Data obtained show that it can be doubled when a milled single crystal is utilized. Transparency of the ceramic particles can be obtained by a future increase of the mother ceramics density to the level of 99%, which will provide its optical transmission to the quality of the single crystal.

Declaration of competing interest

The authors declare that they have no known competing financial interests or personal relationships that could have appeared to influence the work reported in this paper.

Acknowledgement

This work was supported by Russian Federation Government (grant number 14.W03.31.0004). Shared analytical facilities of NRC "Kurchatov institute" - IREA is acknowledged for providing the equipment for materials analysis.

References

[1] V.I. Mikerov, I.A. Zhitnik, J.N. Barmako, E.P. Bogolubov, Prospects for efficient detectors for fast neutron imaging, Appl. Radiat. Isot. 61 (2004) 529–535.

[2] R. Zboray, R. Adams, M. Morgano, Qualification and development of fast neutron imaging scintillator screens, Nucl. Instrum. Methods Phys. Res. A. 930 (2019) 142–150.
[3] N. Kardjilov, M. Dawson, A. Hilger, A highly adaptive detector system for high resolution neutron imaging, Nucl. Instrum. Methods Phys. Res. A. 651 (2011) 95–99.
[4] A. Osovizky, K. Pritchard, J. Ziegler, et al., LiF:ZnS(Ag) mixture optimization for a highly efficient ultrathin cold neutron detector, IEEE Trans. Nucl. Sci. 65 (2018) 1025–1032.
[5] Y. Yehuda-Zada, K. Pritchard, J.B. Ziegler, et al., Optimization of 6LiF:ZnS(Ag) scintillator light yield using GEANT4, Nucl. Instrum. Methods Phys. Res. A 892 (2018) 59–69.
[6] ZnS (Ag), Zinc sulfide scintillation material. Bicron data sheet, Available from: http://www.hep.ph.ic.ac.uk/fets/pepperpot/docs+papers/zns_602.pdf.
[7] NaI(Tl), Polyscin NaI(Tl), Sodium iodide scintillation material. Saint Gobain data sheet, Available from: https://www.crystals.saint-gobain.com/sites/imdf.crystals.com/files/documents/sodium-iodide-material-data-sheet_0.pdf.
[8] P.G. Kontz, G.F. Keepin, Zn(S) Phosphor mixtures for neutron scintillation counting, Los Alamos CIC-14 report reproduction copy LA-1663 (1954) 17.
[9] V.B. Mikhailik, et al., Investigation of luminescence and scintillation properties of ZnS-Ag/6liF scintillator in the 7-295 K temperature range, J. Lumin. 134 (2013) 63–66.
[10] A. Osovizky, K. Pritchard, Y. Yehuda-Zada, et al., Selection of silicon photomultipliers for a 6LiF:ZnS(Ag) scintillator based cold neutron detector, J. Phys. Commun. 2 (2018), 045009.
[11] P. Lecoq, A. Gektin, M. Korzhik, Inorganic Scintillators for Detecting Systems, Springer, 2017.
[12] J. Ueda, S. Tanabe, Review of luminescent properties of Ce3+-doped garnet phosphors: new insight into the effect of crystal and electronic structure, Opt. Mater. X. 1 (2019) 100018–100037.
[13] W.M. Higgins, J. Glodo, E. Van Loef, M. Klugerman, Bridgman growth of LaBr3: Ce and LaCl3: Ce crystals for high-resolution gamma-ray spectrometers, J. Cryst. Growth 287 (2006) 239.
[14] W.M. Higgins, A. Churilov, E. Van Loef, J. Glodo, Crystal growth of large diameter LaBr3: Ce and CeBr3, J. Cryst. Growth 310 (2008) 2085.
[15] N.J. Cherepy, G. Hull, A.D. Drobshoff, S.A. Payne, Strontium and barium iodide high light yield scintillators, Appl. Phys. Lett. 92 (2008), 083508.
[16] Y. Yokota, K. Nishimoto, S. Kurosawa, D. Totsuka, Crystal growth of Eu: SrI2 single crystals by micro-pulling-down method and the scintillation properties, J. Cryst. Growth 375 (2013) 49.
[17] K. Kamada, et al., 2 inch diameter single crystal growth and scintillation properties of Ce:Gd3Al2Ga3O12, J. Cryst. Growth 352 (2012) 88–90.
[18] K. Kamada, et al., Cz grown 2-in. size Ce:Gd3(Al,Ga)5O12 single crystal; relationship between Al, Ga site occupancy and scintillation properties, Opt. Mater. 36 (2014) 1942–1945.
[19] M. Korzhik, V. Alenkov, O. Buzanov, et al., Engineering of a new single-crystal multi-ionic fast and high-light-yield scintillation material (Gd0.5–Y0.5) 3Al2Ga3O12:Ce,Mg, CrystEngComm 22 (2020) 2502–2507.
[20] M. Korzhik, A. Boscovich, A. Fedorov, et al., The scintillation mechanisms in Ce and Tb doped (GdxY1-x) Al2Ga3O12 quaternary garnet structure crystalline ceramics, J. Lumin. 234 (2021) 117933.
[21] Chewpraditkul Weerapong, Scintillation characteristics of Mg2+-codoped Y0.8Gd2.2Al2Ga3O12:Ce single crystal, in: Presented at SCINT2019, 29 September-4 October 2019 (Sendai, Japan).
[22] M. Korjik, V. Alenkov, A. Borisevich, et al., Significant improvement of GAGG: Ce based scintillation detector performance with temperature decrease, Nucl. Instr. and Meth. in Phys. Res. Sect. A Accel. Spectrometers, Detect. Assoc. Equip. 871 (2017) 42–46.
[23] G. Dosovitskiy, P. Karpyuk, E. Gordienko, et al., Neutron detection by Gd-loaded garnet ceramic scintillators, Radiat. Meas. 126 (2019) 106133.
[24] M. Korzhik, Ce doped garnet structure crystalline scintillation materials for HEP instrumentation, J. Inst. Met. 15 (2020) C08001.
[25] M. Korzhik, et al., Compact and effective detector of the fast neutrons on a base of Ce doped Gd3Al2Ga3O12 scintillation crystal, IEEE Trans. Nucl. Sci. 66 (2018) 536–540.
[26] M.P. Taggart, M. Nakohostin, P.J. Sellin, Investigation into the potential of GAGG:Ce as a neutron detector, Nucl. Instrum. Methods Phys. Res. A 931 (2019) 121–126.
[27] A. Fedorov, V. Gurinovich, V. Guzov, et al., Sensitivity of GAGG based scintillation neutron detector with SiPM readout, Nucl. Eng. Tech. 52 (2020) 2306–2312.
[28] TDR 1100-11 Epoxy Adhesive, Advanced materials technical datasheet, Available from: https://us.aralditeadhesives.com/us/adhesives/request-a-tds/228-tdr-1100-11-us-e/file.html.
[29] E. Gordienko, A. Fedorov, E. Radiuk, et al., Synthesis of crystalline Ce-activated garnet phosphor powders and technique to characterize their scintillation light yield, Opt. Mater. 78 (2018) 312–318.
[30] Lithium-6 based screens for detection and imaging of thermal neutrons. Scintacor data sheet, Available from: https://scintacor.com/wp-content/uploads/2015/09/Datasheet-Neutron-Screens-High-Res.pdf.